Clinical value of triple-energy window scatter correction in simultaneous dual-isotope single-photon emission tomography with ^{123}I-BMIPP and ^{201}Tl

Jing-Tao Yang[1], Kazutaka Yamamoto[1], Norihiro Sadato[2], Tatsuro Tsuchida[1], Norio Takahashi[1], Nobushige Hayashi[1], Yoshiharu Yonekura[2], Yasushi Ishii[1]

[1] Department of Radiology, Fukui Medical School, Fukui, Japan
[2] Biomedical Imaging Research Center, Fukui Medical School, Fukui, Japan

Received 10 March and in revised form 17 May 1997

Abstract. To improve the image quality in simultaneous dual-isotope single-photon emission tomography (SPET) with iodine-123 labelled 15-(*p*-iodophenyl)-3-methylpentadecanoic acid (BMIPP) and thallium-201, we applied the triple-energy window method (TEW) for correction of the cross-talk and scatter artifact. Seventy-one patients with coronary artery disease were included. ^{201}Tl cross-talk into the ^{123}I acquisition window (group 1, n = 30) and ^{123}I cross-talk into the ^{201}Tl window (group 2, n = 41) were studied. In group 1, ^{123}I images were first obtained (single-isotope images), followed by ^{201}Tl injection and SPET acquisition using dual-isotope windows (dual-isotope images). In group 2, the order was reversed. The dual-isotope SPET images with and without TEW were compared with the single-isotope images. Qualitative evaluation was performed by scoring the segmental defect pattern. Detectability of the mismatched fatty acid metabolism on dual-isotope SPET was evaluated by receiver operating characteristic (ROC) curve analysis. Segmental defect pattern agreement between dual and corrected single images was significantly improved by TEW correction (P<0.01). The agreement was particularly improved in segments with absence of uptake. There was no significant difference between TEW-corrected dual-isotope SPET and corresponding single-isotope SPET with regard to either % defect count or background activity. Mismatched fatty acid metabolism depicted by dual-isotope SPET predicted abnormal wall motion more accurately with TEW than without TEW. With TEW, a practical method for scatter and cross-talk correction in clinical settings, simultaneous dual ^{123}I-BMIPP/^{201}Tl SPET is feasible for the assessment of myocardial perfusion/metabolism mismatch.

Correspondence to: Jing-Tao Yang, Department of Radiology, Fukui Medical School, 23-3 Shimoaizuki, Matsuoka-Cho, Yoshida-Gun, Fukui, 910-11, Japan

Key words: Dual-isotope single-photon emission tomography – Triple-energy window method – Iodine-123 BMIPP – Thallium-201 – Coronary artery disease

Eur J Nucl Med (1997) 24:1099–1106

Introduction

Iodine-123 labelled 15-(*p*-iodophenyl)-3-methylpentadecanoic acid (BMIPP) has unique metabolic properties for the assessment of myocardial fatty acid metabolism [1, 2]. Mismatch in the distribution of ^{123}I-BMIPP compared with that of thallium-201 has been reported in various myocardial diseases [3–17]. The mismatch typically indicates more severely impaired fatty acid metabolism than coronary perfusion. In ischaemic heart, a discordant decrease in ^{123}I-BMIPP uptake was frequently seen in areas showing left ventricular dysfunction with preserved perfusion [11]. These areas of discordant decrease in ^{123}I-BMIPP uptake also showed a discordant increase in glucose accumulation whereas perfusion and oxidative metabolism were preserved [17], indicating that they represented ischaemic but viable myocardium. Thus, combined assessment using ^{123}I-BMIPP and ^{201}Tl might contribute to better understanding of the pathogenesis and tissue viability of various cardiac disorders [8–18].

Simultaneous dual-isotope single-photon emission tomography (SPET) using ^{123}I-BMIPP and ^{201}Tl would be of considerable clinical value if the radioactivity can be reliably separated. Simultaneous data acquisition permits quantification of the mismatch on a pixel-by-pixel basis, avoiding misregistration. Simultaneous measurement is essential for the evaluation of acute coronary disorders, in which pathophysiological conditions may alter quickly. However, dual-isotope imaging can be misinterpreted due to Compton scatter and radionuclide cross-talk artifacts [19–22].

The triple-energy window method (TEW) was proposed by Ogawa et al. [23]. They set two subwindows on each side of the main photopeak window. Scatter events in the main window are estimated by averaging the projections from the subwindows. TEW can accurately compensate for Compton scatter, contributing significantly to quantitative analysis in single- and dual-isotope SPET studies [24, 25]. In the clinical practice of single-isotope SPET, TEW has proved effective by improving the image contrast and quantification [26, 27]. Phantom studies have also suggested that TEW is a promising method for the effective separation of two radionuclides in dual-isotope SPET [26, 28].

In this study, we applied TEW for simultaneous dual-isotope SPET with ^{123}I-BMIPP and ^{201}Tl in clinical settings, examining its effectiveness in scatter and cross-talk correction. We further examined its effect on the detection of mismatched fatty acid metabolism.

Materials and methods

Patient population and protocol design. A total of 71 patients with coronary artery disease were studied (Table 1). Patients were separated into two groups in which different imaging protocols were used. The correction of ^{201}Tl cross-talk into the ^{123}I-BMIPP acquisition window was studied in 30 patients (group 1). They were first examined with 111 MBq (3 mCi) of ^{123}I-BMIPP. Then, 111 MBq (3 mCi) of ^{201}Tl was injected at rest, followed by SPET acquisition using dual-isotope energy windows 10 min later (Fig. 1A). Comparison of dual-isotope SPET ^{123}I-BMIPP images with single-isotope SPET ^{123}I images was performed in this group.

The other 41 patients (group 2) were studied to assess the correction of ^{123}I-BMIPP cross-talk into the dual-isotope ^{201}Tl window. Stress and delayed single-isotope ^{201}Tl images were first obtained. Patients underwent graded bicycle exercise, ^{201}Tl chloride (111 MBq) being injected at peak exercise followed by stress

Table 1. Subject information

	Group 1	Group 2
Age (mean±SD)	64.5±5.7	63.2±6.8
Gender (men/women)	26/4	35/6
Myocardial infarction	21	25
Angina pectoris	9	16

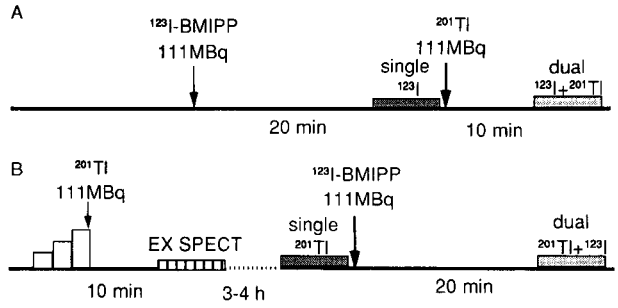

Fig. 1. Schematic drawing of the imaging protocols used for group 1 (**A**) and group 2 (**B**)

^{201}Tl SPET scan 10 min later, and delayed ^{201}Tl SPET scan 3–4 h later. Then ^{123}I-BMIPP (111 MBq) was injected. SPET acquisition was performed 20 min later using dual-isotope windows (Fig. 1B). Dual-isotope SPET ^{201}Tl images were compared with delayed single-isotope SPET ^{201}Tl images. All patients gave their informed consent before participating in the study. The study protocol was approved by the local ethical review committee.

For clarity of nomenclature, the single-isotope SPET ^{123}I-BMIPP images with TEW correction will be referred to as single ^{123}I TEW(+), and those without TEW correction as single ^{123}I TEW(–). Similar abbreviations used in the text are summarized in Table 2.

SPET imaging techniques. SPET acquisition was performed using a triple-head, rotating gamma camera (GCA-9300A/HG: Toshiba, Japan) equipped with low-energy, high-resolution, parallel-hole collimators. All patients were carefully positioned in the same location for corresponding single- and dual-isotope SPET acquisition. The images were acquired in continuous rotational motion composed of 90 angular samples framed into 4° intervals with a 64×64 matrix for a total imaging time of 15 min. The photopeak and main windows used for data acquisition in ^{201}Tl imaging were 71 keV and 24%, respectively, and for ^{123}I imaging, 160 keV and 26%, respectively. For TEW, the two subwindows of 3% on both sides of the main windows were set for each photopeak. The projection images acquired by the main window and subwindow were initially smoothed with a Butterworth filter of order 8, and cut-off frequencies for the main window and the subwindow were 0.3 and 0.1 cycles/pixel, respectively. Image reconstruction was based on filtered backprojection with a ramp filter. Reconstructed transverse slices covered the left ventricular myocardium. These images were further processed to obtain vertical long-axis, horizontal long-axis and short-axis slices. For single- and dual-isotope acquisition data, the same reconstruction of tomographic images was performed. Attenuation correction was not performed.

Table 2. List of abbreviations

Abbreviation	Definition
Single ^{123}I TEW(+)	Single-isotope SPET ^{123}I-BMIPP images with TEW correction
Single ^{123}I TEW(–)	Single-isotope SPET ^{123}I-BMIPP images without TEW correction
Dual ^{123}I TEW(+)	Dual-isotope SPET ^{123}I-BMIPP images with TEW correction
Dual ^{123}I TEW(–)	Dual-isotope SPET ^{123}I-BMIPP images without TEW correction
Single ^{201}Tl TEW(+)	Delayed single SPET ^{201}Tl images with TEW correction
Single ^{201}Tl TEW(–)	Delayed single SPET ^{201}Tl images without TEW correction
Dual ^{201}Tl TEW(+)	Dual-isotope SPET ^{201}Tl images with TEW correction
Dual ^{201}Tl TEW(–)	Dual-isotope SPET ^{201}Tl images without TEW correction

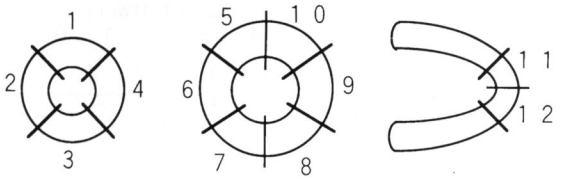

Fig. 2. Schematic representation of 12 segments on two short-axis slices and one vertical long-axis slice. Severity score: 4 = absence of uptake, 3 = severely reduced uptake, 2 = moderately reduced uptake, 1 = mildly reduced uptake and 0 = normal uptake

Visual evaluation of TEW correction. For visual interpretation, all SPET images with TEW were displayed with the intensity of each image normalized to the maximal pixel value in that image as 100% and a cutoff level of 0%, whereas for images without TEW, a cutoff level of 10% was chosen to minimize the background activity on the display. Corresponding single TEW(+) and dual TEW(+) or TEW(–) SPET images were visually evaluated by two experienced nuclear medicine physicians blindly without clinical and technical information. The left ventricular myocardium was divided into 12 segments as shown in Fig. 2 and reduced uptake in each segment was scored with a five-point grading system (4 = absence of uptake, 3 = severely reduced uptake, 2 = moderately reduced uptake, 1 = mildly reduced uptake and 0 = normal uptake). Segmental score agreement rates of dual TEW(+) and dual TEW(–) with single TEW(+) were calculated.

Quantitative analysis of TEW correction. To evaluate the effect of TEW on the defect and left ventricular cavity background activity, the line profile curve across the lesion was obtained as follows. First, a short-axis slice with maximal defect was manually selected from single-isotope SPET images. A corresponding dual-isotope SPET short-axis slice was selected using a computerized semi-automatic algorithm to eliminate inter-observer discrepancy and to maximize inter-study reproducibility. A line profile curve that passed through the centre of the left ventricle and defect was created on the same position on each corresponding short-axis slice. The counts in the myocardial region opposite to the defect (myocardial counts), in the left ventricular cavity (LV counts) and in the defect region (defect counts) on the line profile curve were obtained (Fig. 3). The relative radioactivity in the defect (% defect count) was determined as the ratio of the defect counts to the myocardial counts, and the % LV count was calculated as the ratio of the LV counts to the myocardial counts for each image.

$$\%\ \text{defect count} = \frac{\text{defect count}}{\text{myocardial count}} \times 100\ (\%) \quad (1)$$

$$\%\text{LV count} = \frac{\text{LV count}}{\text{myocardial count}} \times 100\ (\%) \quad (2)$$

To quantify the mismatch between myocardial perfusion and fatty acid metabolism on dual-isotope SPET, circumferential profile curves were generated from apical to basal short-axis slices to create a bull's-eye polar map of % myocardial tracer uptake, in which a maximum count was normalized as 100%. The analysis was performed with nine regions of interest placed on each polar map and the relative count (%count) of each myocardial segment was obtained (Fig. 4). The Mismatch Index between ^{201}Tl and ^{123}I-BMIPP was calculated as follows:

Mismatch Index of TEW(–)
= %count of dual ^{201}Tl TEW(–)–%count of dual ^{123}I TEW(–) (3)

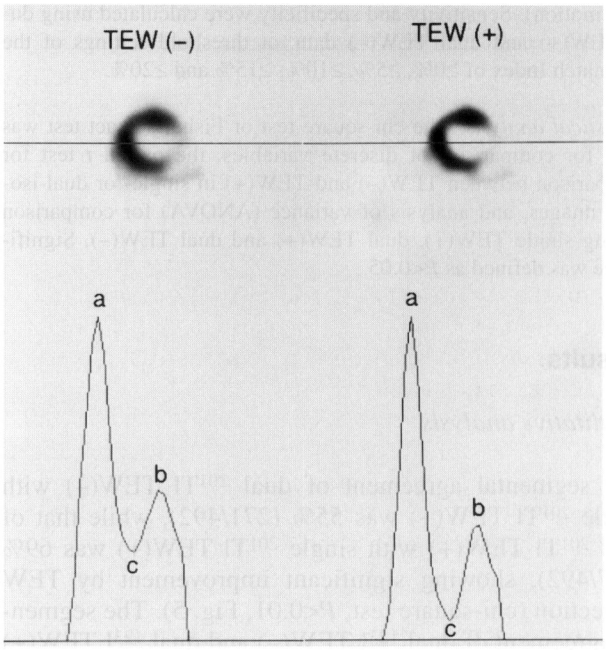

Fig. 3. Line profile curve analysis on selected ^{123}I-BMIPP short-axis images. *Left*: image without TEW. *Right*: image with TEW. *a*, Normalized myocardial count, *b*, normalized defect count; *c*, normalized LV count. Note that the decrease in the %LV count with TEW correction is larger than that in the %defect count

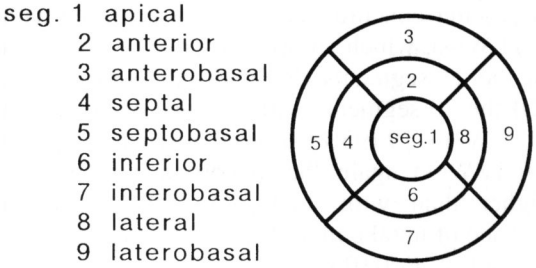

Fig. 4. Schema of nine myocardial segments on the bull's-eye map

Mismatch Index of TEW(+)
= %count of dual ^{201}Tl TEW(+)–%count of dual ^{123}I TEW(+) (4)

Regional wall motion analysis. Left ventriculography and echocardiography were performed for each subject within 6 weeks of myocardial imaging. The wall motion was evaluated by consensus of two cardiologists who were blinded to the SPET results. Wall motion of nine segments (anterobasal, anterior, apical, inferior, inferobasal, septal, septobasal, lateral and laterobasal) was categorized as normal, hypokinesis, akinesis, or dyskinesis [29]. As segments with mismatched perfusion and fatty acid metabolism are known to show abnormal wall motion [11], receiver operating characteristic (ROC) curve analysis [30] was performed to evaluate the extent to which abnormal wall motion could be predicted by mismatched fatty acid metabolism. Mismatched fatty acid metabolism was evaluated by the Mismatch Index. Sensitivity was defined as: (number of segments with mismatched fatty acid metabolism)/(number of segments with abnormal wall motion). Specificity was defined as: (number of segments without mismatched fatty acid metabolism)/(number of segments with normal

wall motion). Sensitivity and specificity were calculated using dual TEW(+) and dual TEW(–) data, at threshold settings of the Mismatch Index of ≥0%, ≥5%, ≥10%, ≥15% and ≥20%.

Statistical analysis. The chi-square test or Fisher's exact test was used for comparison of discrete variables, the paired *t* test for comparison between TEW(–) and TEW(+) in single- or dual-isotope images, and analysis of variance (ANOVA) for comparison among single TEW(+), dual TEW(+) and dual TEW(–). Significance was defined as $P<0.05$.

Results

Qualitative analysis

The segmental agreement of dual ^{201}Tl TEW(–) with single ^{201}Tl TEW(+) was 55% (271/492), while that of dual ^{201}Tl TEW(+) with single ^{201}Tl TEW(+) was 69% (337/492), showing significant improvement by TEW correction (chi-square test, $P<0.01$, Fig. 5). The segmental agreement of dual ^{123}I TEW(–) and dual ^{123}I TEW(+) with single ^{123}I TEW(+) was 63% (226/360) and 75% (271/360) respectively, again with significant improvement by TEW correction (chi-square test, $P<0.01$, Fig. 6). Of the 21 segments with absence of uptake (score 4) on single ^{201}Tl TEW(+), 18 (86%) showed absence of uptake on dual ^{201}Tl TEW(+); this represents significantly better concordance than was achieved with dual ^{201}Tl TEW(–), which showed absence of uptake in only 12 of the 21 segments (57%; Fisher' s exact test, $P<0.05$). Of the 20 segments with absence of uptake on single ^{123}I TEW(+), 19 (95%) showed absence of uptake on dual ^{123}I TEW(+), again, the concordance was significantly higher than with dual ^{123}I TEW(–), which showed absence of uptake in 9 of the 20 segments (45%; Fisher' s exact test, $P<0.01$).

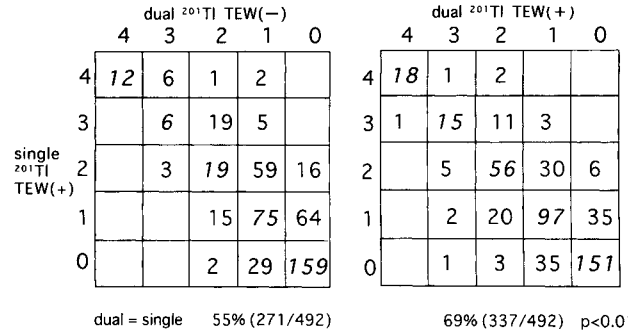

Fig. 5. Segmental score agreement between single ^{201}Tl TEW(+) and dual ^{201}Tl images without [TEW(–)] and with [TEW(+)] TEW correction

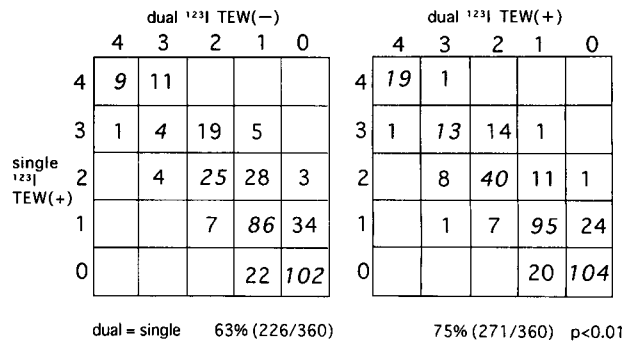

Fig. 6. Segmental score agreement between single ^{123}I-BMIPP TEW(+) and dual ^{123}I-BMIPP images without [TEW(–)] and with [TEW(+)] TEW correction

Quantitative analysis

Background activity. Compared with single TEW(–) images,%LV count and %defect count were significantly lower for both ^{201}Tl and ^{123}I-BMIPP on single TEW(+) images (paired *t* test, $P<0.01$; Table 3, Fig. 7). The %LV count and %defect count were also significantly lower on dual TEW(+) images compared with dual TEW(–) images (paired *t* test, $P<0.01$; Table 3). There was no significant difference between single TEW(+) and dual TEW(+) (ANOVA test; Fig. 8); hence better contrast between myocardium and LV cavity or myocardial defects is achieved with single TEW(+) and dual TEW (+) than with dual TEW (–) images.

Detection of mismatched fatty acid metabolism. The Mismatch Index of dual TEW(+) showed a high correlation with that of dual TEW(–) in both group 1 ($y =$

Table 3. Comparison of %LV count and %defect count between (a) single TEW(–) and single TEW(+) and (b) dual TEW(–) and dual TEW(+)

	^{201}Tl (n=41; mean± SD)		^{123}I (n=30; mean± SD)	
	TEW(–)	TEW(+)	TEW(–)	TEW(+)
a) *Single TEW(–) and single TEW(+)*				
%LV count	31.8±10.5	10.8±8.11*	39.5±9.68	21.2±8.57*
%Defect count	58.3±14.2	49.0±15.2*	57.2±11.0	47.4±14.5*
b) *Dual TEW(–) and dual TEW(+)*				
%LV count	44.2±10.1	14.5±9.5*	42.1±8.7	21.0±9.8*
%Defect count	65.9±10.9	53.4±13.7*	62.6±11.9	51.0±15.5*

* $P<0.01$ vs TEW(–)

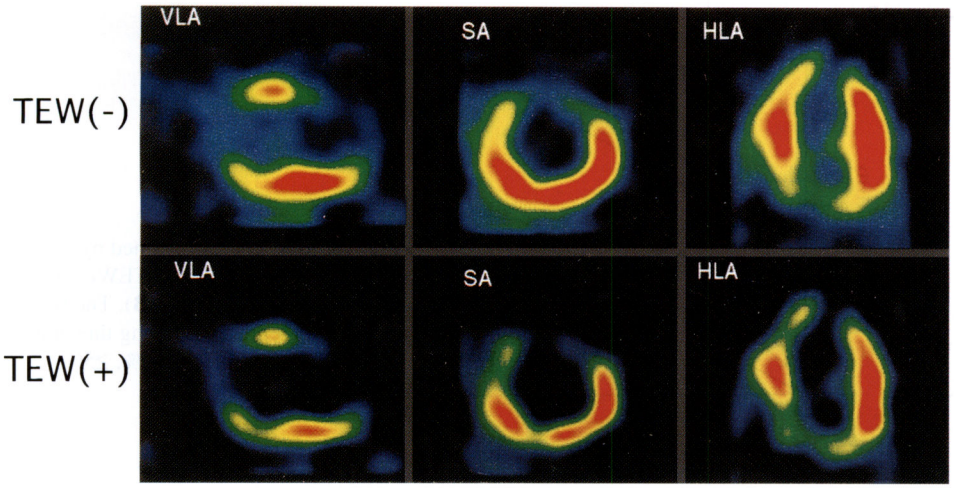

Fig. 7. Single-isotope SPET ^{201}Tl images of a 44-year-old man with old anteroseptal myocardial infarction. Coronary arteriogram revealed total occlusion of LAD#6, and 80% stenosis of RCA#4. Left ventriculogram showed akinesis of the anterior, apical and septal wall, and hypokinesis of the inferior wall. Note that images with TEW had clear defects of the septal and inferior wall. *VLA*, Vertical long-axis; *SA*, short-axis; *HLA*, horizontal long-axis

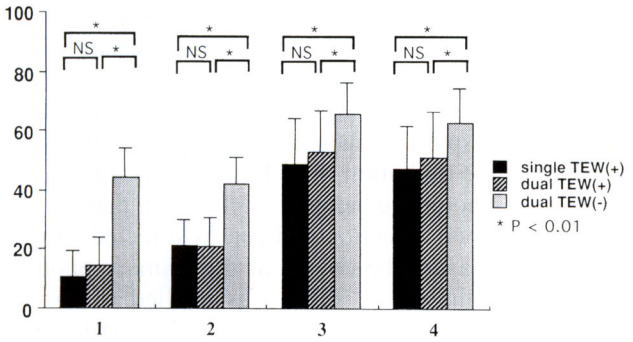

Fig. 8. Comparison of the %LV count and %defect count on single TEW(+), dual TEW(+) and dual TEW(–). *1*, %LV count of ^{201}Tl; *2*, %LV count of ^{123}I; *3*, %defect count of ^{201}Tl; *4*, %defect count of ^{123}I

Table 4. Comparison of regional wall motion with Mismatch Index of dual TEW(–) and dual TEW(+) in groups 1 and 2

Wall motion	Dual TEW(–)			Dual TEW(+)		
	≤–10%	–10% ~10%	≥10%	≤–10%	–10% ~10%	≥10%
In group 1						
Normal	13	140	4	32	119	6
Abnormal	3	88	22	5	66	42
Total	16	228	26	37	185	48
In group 2						
Normal	10	167	3	37	139	4
Abnormal	3	151	35	5	120	64
Total	13	318	38	42	259	68

–0.87+1.21 x; r = 0.86) and group 2 (y = –1.33+1.23 x; r = 0.84) (Fig. 9). The slope of the regression lines showed that the absolute value of the Mismatch Index with TEW is approximately 20% higher than that without TEW.

The ROC curves showed that dual TEW(+) predicted abnormal wall motion by mismatched fatty acid metabolism better than did dual TEW(–) (Fig. 10). The results using a Mismatch Index threshold absolute value of ≥10% are given in Table 4. TEW increased sensitivity (abnormal wall motion with Mismatch Index ≥10%) from 19% (22/113) to 37% (42/113) in group 1, and from 18% (35/189) to 34% (64/189) in group 2, while specificity (normal wall motion without Mismatch Index ≥10%) was almost unchanged in both groups (in group

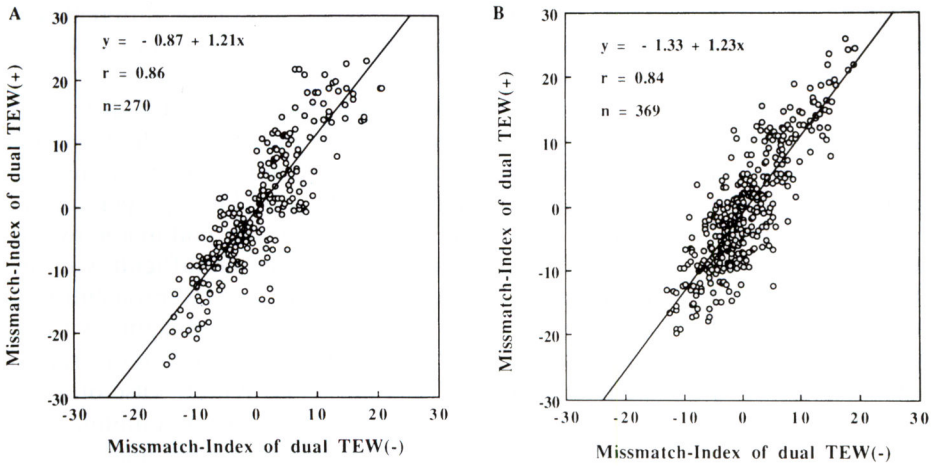

Fig. 9. Correlation between the Mismatch Index of dual TEW(+) and dual TEW(–) in group 1 (**A**) and group 2 (**B**)

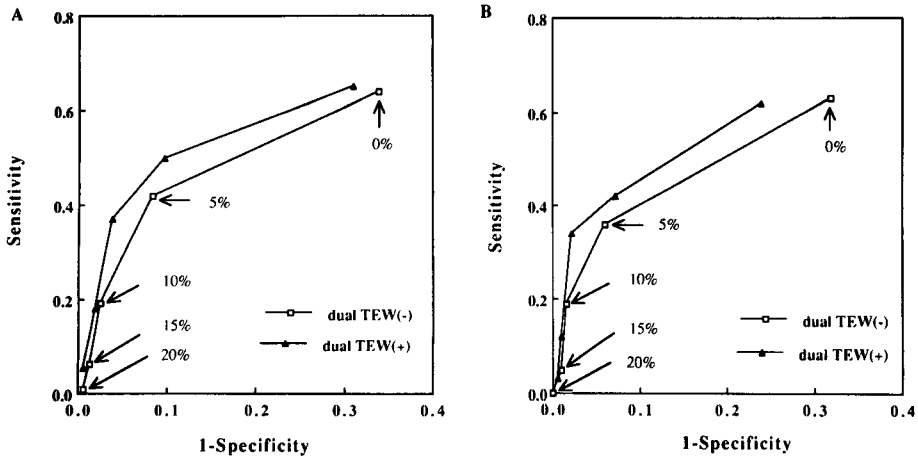

Fig. 10. ROC curves obtained by means of dual TEW(+) and dual TEW(–) in group 1 (**A**) and group 2 (**B**). The five data points represent varying thresholds of the Mismatch Index: ≥0%, ≥5%, ≥10%, ≥15% and ≥20%

1: 97% before TEW, 96% afterwards; in group 2: 98% before TEW, 98% afterwards). On the other hand, in group 1 the percentage of segments with a Mismatch Index of ≤–10% was increased from 5.9% (16/270) to 14% (37/270) by TEW, and in group 2 it was increased from 3.5% (13/369) to 11% (42/369). Of these segments, 68% (25/37) were located in the septum and inferior wall in group 1, as compared with 76% (32/42) in group 2. There was no difference in mismatch distribution between group 1 (BMIPP/rest Tl) and group 2 (BMIPP/delayed Tl).

Discussion

A potential problem with simultaneous dual-isotope SPET is the cross-talk photon contribution from one radionuclide to a second radionuclide' s photopeak energy window. The cross-talk depends on many factors, including radionuclide energies, object sizes, differences in tracer distribution, and uptake by surrounding organs such as liver and lung [31–33]. Hence, complicated problems caused by Compton scattering and cross-talk are anticipated in clinical studies. Most corrections applied in simultaneous dual-isotope imaging are based on the simple cross-talk correction method used in dual-radionuclide in vitro counting [34, 35]; others are based on offset photopeak image acquisition and ignore the cross-talk between windows [36, 37]. However, the cross-talk components are not eliminated by using asymmetric windows [38], and the simple cross-talk correction method does not account for the differences in spatial distribution of the photons recorded in the cross-talk window and the primary photopeak window [38–40]. A study using dual-isotope ^{123}I/^{201}Tl to evaluate the influence of cross-talk in phantoms and patients demonstrated that the cross-talk of ^{123}I and ^{201}Tl to the other energy window varied from case to case and that the fraction of cross-talk differed with time after injection, suggesting that the fraction of cross-talk obtained from phantoms by simple cross-talk correction method is not directly applicable in clinical settings [22]. Thus, cross-talk correction based on in vivo measurement is necessary for quantitative and qualitative dual-isotope SPET imaging.

In this study, we used the scatter-corrected single-isotope SPET images as a "gold standard" to investigate the effect of cross-talk and scatter correction. This approach is justifiable despite the lack of knowledge of true values, which is the limitation of a clinical study. In clinical settings, the photons generated within the patient are scattered, and their direction and energy affected. Hence it is hard to measure the counts of the primary photons accurately. In this study, TEW was applied to correct both scatter and cross-talk. TEW has been validated as a method to improve the quantification and contrast of single-isotope SPET by elimination of the scatter component [23–27]. Hence it is reasonable to use single-isotope SPET with TEW correction as a reference to validate the efficacy of TEW for the correction of both scatter and cross-talk in dual-isotope SPET.

Dual TEW(–) tended to underestimate the decrease in tracer uptake in approximately 50% of segments with absence of uptake (score of 4) in both ^{123}I-BMIPP and ^{201}Tl images (Figs 5, 6). As this implies that an area of score 4 would be misinterpreted as having a score of 3, 2 or 1, the evaluation of fatty acid metabolism/flow mismatch would be biased without cross-talk correction. In contrast, a high agreement (approximately 90%) was obtained in respect of such segments (score of 4) with dual TEW(+). Thus dual TEW(+) accurately differentiated between defects with absence of uptake (score of 4) and defects with reduced uptake (score of 3, 2 or 1).

Despite TEW correction, there were still disparities with regard to some segments in corresponding corrected single-isotope and dual-isotope images. Such disparities may be caused by two factors: First, proper correction of lead X-rays produced in the collimator by the high-energy photons from ^{123}I may be difficult with the TEW method. Second, ^{201}Tl has an 11% probability of emitting a 167-keV photon; hence, the imaging window set for ^{123}I-BMIPP (160 keV) will also partially record the photopeak (167-keV) of ^{201}Tl. With the use of a different collimator, it may be possible to minimize the contribution of lead X-rays in dual-isotope imaging [41,

42]. It is noteworthy that although the TEW method seems to give promising results for dual $^{123}I/^{201}Tl$ imaging, other combinations of radioisotopes may be much more difficult to deal with, e.g. ^{123}I and ^{99m}Tc, because of the proximity of the photopeak locations for the radioisotopes [26].These limitations of TEW correction should be kept in mind when applying it in clinical settings.

TEW reduced background activity, as shown by quantitative analysis. This effect was more prominent in the LV cavity than in the myocardial defect, underscoring the characteristics of TEW. As a method of position-dependent scatter compensation, TEW has an advantage over conventional scatter and cross-talk correction, such as simple low cutoff subtraction and the simple cross-talk correction method. Furthermore, among several methods which yield similarly good scatter correction, TEW is the easiest method to implement on a routine basis [43, 44].

ROC analysis was performed in order to evaluate the prediction of abnormal wall motion – confirmed by left ventriculography and echocardiography – by mismatched fatty acid metabolism detected on dual-isotope SPET. This approach is reasonable, as dysfunctional myocardium such as hibernating and stunned myocardium often shows mismatched fatty acid metabolism [11]. ROC curves showed that dual TEW(+) predicted abnormal wall motion better than did dual TEW(–), mainly due to the increased Mismatch Index values in dysfunctional myocardium.

The number of segments with higher ^{123}I-BMIPP uptake than ^{201}Tl uptake increased on dual TEW(+), probably due to the difference in attenuation between the radionuclides. As the photon energy of ^{123}I is higher than that of ^{201}Tl, the attenuation of ^{123}I is substantially lower than that of ^{201}Tl, particularly in septal and inferior regions. As scatter correction was performed without attenuation compensation in this study, the ^{123}I-BMIPP $>^{201}Tl$ type mismatch might have been enhanced in the septum and the inferior wall on dual TEW(+). An appropriate attenuation correction may compensate for this kind of artifact.

References

1. Knapp FF Jr, Goodman MM, Callahan AP, Kirsch G. Radioiodinated 15-(*p*-iodophenyl)-3,3-dimethylpentadecanoic acid: a useful new agent to evaluate myocardial fatty acid uptake. *J Nucl Med* 1986; 27: 521–531.
2. Ambrose KR, Owen BA, Goodman MM, Knapp FF Jr. Evaluation of the metabolism in rat hearts of two new radioiodinated 3-methyl-branched fatty acid myocardial imaging agents. *Eur J Nucl Med* 1987; 12: 486–491.
3. Yonekura Y, Brill AB, Som P, et al. Regional myocardial substrate uptake in hypertensive rats: a quantitative autoradiographic measurement. *Science* 1985; 227: 1494–1496.
4. Yamamoto K, Som P, Brill AB, et al. Dual-tracer autoradiographic study of beta-methyl-(I-^{14}C) heptadecanoic acid and 15-*p*-(^{131}I)-iodophenyl-beta-methyl pentadecanoic acid in normotensive and hypertensive rats. *J Nucl Med* 1986; 27: 1178–1183.
5. Kurata C, Kobayashi A, Yamazaki N. Dual-tracer autoradiographic study with thallium-201 and radioiodinated fatty acid in cardiomyopathic hamsters. *J Nucl Med* 1989; 30: 80–87.
6. Miller DD, Gill JB, Livni E, et al. Fatty acid analogue accumulation: a marker of myocyte viability in ischemic reperfused myocardium. *Circ Res* 1988; 63: 681–692.
7. Nishimura T, Sago M, Kihara K, et al. Fatty acid myocardial imaging using ^{123}I-—methyl-iodophenyl pentadecanoic acid (BMIPP): comparison of myocardial perfusion and fatty acid utilization in canine myocardial infarction (occlusion and reperfusion model). *Eur J Nucl Med* 1989; 15: 341–345.
8. Strauss HW, Yasuda T, Gold HK, et al. Potential role of combined fatty acid and thallium imaging in patients with myocardial ischemia and infarction [abstract]. *J Nucl Med* 1987; 28: 632.
9. Vyska K, Machulla HJ, Stremmel W, et al. Regional myocardial free fatty acid extraction in normal and ischemic myocardium. *Circulation* 1988; 78: 1218–1233.
10. Kurata C, Tawarahara K, Taguchi T, et al. Myocardial emission computed tomography with iodine-123-labeled beta-methyl-branched fatty acid in patients with hypertrophic cardiomyopathy. *J Nucl Med* 1992; 33: 6–13.
11. Tamaki N, Kawamoto M, Yonekura Y, et al. Regional metabolic abnormality in relation to perfusion and wall motion in patients with myocardial infarction: assessment with emission tomography using an iodinated branched fatty acid analog. *J Nucl Med* 1992; 33: 659–667.
12. Nishimura T, Uehara T, Shimonagata T, Nagata S, Haze K. Clinical results with β-methyl-*p*-(^{123}I) iodophenylpentadecanoic acid, single-photon emission computed tomography in cardiac disease. *J Nucl Cardiol* 1994; 1: s65–s71.
13. Kawamoto M, Tamaki N, Yonekura Y, et al. Combined study with I-123 fatty acid and thallium-201 to assess ischemic myocardium: comparison with thallium redistribution and glucose metabolism. *Ann Nucl Med* 1994; 8: 47–54.
14. Takeishi Y, Chiba J, Abe S, Tonooka I, Komatani A, Tomoike H. Heterogeneous myocardial distribution of iodine-123 15-(*p*-iodophenyl)-3-*R,S*-methylpentadecanoic acid (BMIPP) in patients with hypertrophic cardiomyopathy. *Eur J Nucl Med* 1992; 19: 775–782.
15. Saito T, Yasuda T, Gold HK, et al. Differentiation of regional perfusion and fatty acid uptake in zones of myocardial injury. *Nucl Med Commun* 1991; 12: 663–675.
16. Tawarahara K, Kurata C, Taguchi T, et al. Simultaneous dual myocardial imaging with iodine-123-—methyl iodophenylpentadecanoic acid (BMIPP) and thallium-201 in patients with coronary heart disease. *Jpn Circ J* 1994; 58: 107–115.
17. Tamaki N, Tadamura E, Kawamoto M, et al. Decreased uptake of iodinated branched fatty acid analog indicates metabolic alterations in ischemic myocardium. *J Nucl Med* 1995; 36: 1974–1980.
18. Knapp FF Jr, Kropp J. Iodine-123-labelled fatty acids for myocardial single-photon emission tomography: current status and future perspectives. Eur *J Nucl Med* 1995; 22: 361–381.
19. Weinstein H, King MA, Reinhardt CP, McSherry B, Leppo JA. A method of simultaneous dual radionuclide cardiac imaging with ^{99m}Tc and ^{201}Tl. Part I. Analysis of inter-radionuclide crossover and validation in phantoms. *J Nucl Cardiol* 1994; 1: 39–51.
20. Kiat H, Germano G, Van Train K, et al. Quantitative assessment of photon spillover in simultaneous rest Tl-201/stress

Tc-99m sestamibi dual-isotope myocardial perfusion SPET [abstract]. *J Nucl Med* 1992; 33: 854–855.
21. Kiat H, Germano G, Friedman J, et al. Comparative feasibility of separate or simultaneous rest thallium-201/stress technetium-99m-sestamibi dual-isotope myocardial perfusion SPET. *J Nucl Med* 1994; 35: 542–548.
22. Nakajima K, Taki J, Bunko H, et al. Error of uptake in dual energy acquisition with ^{201}Tl and ^{123}I labeled radiopharmaceuticals. *Eur J Nucl Med* 1990; 16: 595–599.
23. Ogawa K, Harata Y, Ichihara T, Kubo A, Hashimoto S. A practical method for position-dependent Compton scatter compensation in single photon emission CT. *IEEE TMI* 1991; 10: 408–412.
24. Ichihara T, Ogawa K, Motomura N, Kubo A, Hashimoto S. Compton scatter compensation using the triple-energy window method for single- and dual-isotope SPET. *J Nucl Med* 1993; 34: 2216–2221.
25. Ogawa K. Simulation study of triple-energy-window scatter correction in combined Tl-201,Tc-99m SPET. *Ann Nucl Med* 1994; 8: 277–281.
26. Nakajima K, Matsudaira M, Yamada M, Taki J, Tonami N, Hisada K. Effect of scatter correction on quantification of myocardial SPET and application to dual-energy acquisition using triple-energy window method. *Jpn J Nucl Med* 1995; 32: 959–967.
27. Iida H, Takahashi M, Motomura N, Hachiya T, Nakagawara J. Effects of Compton scatter in quantitative brain SPET. *Jpn J Nucl Med* 1996; 33: 143–151.
28. Cullom SJ, Jones ME. An experimental evaluation of TEW scatter compensation for spectral crossover in simultaneous Tl-201/Tc-99m-MIBI SPET [abstract]. *J Nucl Med* 1995; 36: 168.
29. Blanksma PK, Willemsen ATM, Meeder JG et al. Quantitative myocardial mapping of perfusion and metabolism using parametric polar map displays in cardiac PET. *J Nucl Med* 1995; 36: 153–158.
30. Metz CE. ROC methodology in radiographic imaging. *Invest Radiol* 1986; 21: 720–733.
31. Floyd CE, Jaszczak RJ, Harris CC, Coleman RE. Energy and spatial distribution of multiple order Compton scatter in SPET: a Monte Carlo simulation. *Phys Med Biol* 1984; 29: 1217–1230.
32. Budinger TF, Rollo D. Physics and instrumentation. In: Holman BL, Sonnenblick EH, Lesch M, eds. *Principles of cardiovascular nuclear medicine*. New York: Grune and Stratton; 1978: 17–52.
33. DePuey EG. Simultaneous thallium-201/technetium-99m dual-isotope cardiac SPET: ready for prime time? [editorial]. *J Nucl Med* 1993; 34: 2006–2008.
34. Neumann DR. Simultaneous dual-isotope SPET imaging for the detection and characterization of parathyroid pathology. *J Nucl Med* 1992; 33: 131–134.
35. Juni JE, Bernstein RC, Ponto RA, Nuechterlein PM. Simultaneous dual-tracer brain SPET with Tc-99m HMPAO and I-123 iodoaphetamine – method and validation [abstract]. *J Nucl Med* 1991; 32: 956.
36. Devous MD Sr., Payne JK, Lowe JL. Dual-isotope brain SPET imaging with Tc-99m and I-123: clinical validation using Xe-133 SPET. *J Nucl Med* 1992; 33: 1919–1924.
37. Devous MD Sr, Lowe JL, Payne JK. Dual-isotope brain SPET imaging with Tc-99m and I-123: validation by phantom studies. *J Nucl Med* 1992; 33: 2030–2035.
38. Ivanovic M, Weber DA, Loncaric S, Franceschi D. Feasibility of dual radionuclide brain imaging with I-123 and Tc-99m. *Med Phys* 1994; 21: 667–674.
39. Knesaurek K. A new dual-isotope convolution cross-talk correction method: a Tl-201/Tc-99m SPET cardiac phantom study. *Med Phys* 1994; 21: 1577–1583.
40. Frey EC, Tsui BMW, Perry JR. Simultaneous acquisition of emission and transmission data for improved thallium-201 cardiac SPET imaging using a technetium-99m transmission source. *J Nucl Med* 1992; 33: 2238–2245.
41. Moore SC, Zimmerman RE, Chan KH, English RJ, Kijewski MF. Experimental and Monte Carlo characterization of spectral and spatial distributions of lead x-rays [abstract]. *J Nucl Med* 1994; 35: 61.
42. Moore SC, English RJ, Syravanh C, Tow DE, Zimmerman RE, Chan KH, Kijewski MF. Simultaneous Tc-99m/Tl-201 imaging using energy-based estimation of the spatial distributions of contaminant photons. *IEEE Trans Nucl Sci* 1995; 42: 1189–1195.
43. Ljungberg M, King MA, Hademenos GJ, Strand SE. Comparison of four scatter correction methods using Monte Carlo simulated source distributions. *J Nucl Med* 1994; 35: 143–151.
44. Buvat I, Rodriguez-Villafuerte M, Todd-Pokropek A, Benali H, Di Paola R. Comparative assessment of nine scatter correction methods based on spectral analysis using Monte Carlo simulations. *J Nucl Med* 1995; 36: 1476–1488.